

Correlation properties of large and small-scale parameters from multicell channel measurements

(Invited Paper)

S. Jaeckel, L. Jiang, V. Jungnickel, L. Thiele

Fraunhofer Inst. for Telecommunications
Heinrich Hertz Institut
D-10587 Berlin, Germany

C. Jandura

Technical University Dresden
Vodafone Chair
D-01062 Dresden, Germany

G. Sommerkorn, C. Schneider

Ilmenau University of Technology
Inst. of Information Technology
D-98684 Ilmenau, Germany

Abstract—Based on two multicell measurement campaigns in Berlin and Dresden, correlation properties for channel parameters to different sites and to adjacent sectors of the same site are investigated. Results indicate that the assumptions in the widely used 3GPP spatial channel model (SCM) form an upper bound for the multicell correlations compared to our measurements. If the SCM is used to evaluate the performance of novel cooperative base station techniques, simulation results regarding the throughput can be considered as a lower bound for the capacity achievable in our measurement scenarios.

Index Terms—radio propagation, channel sounding, antenna arrays, cooperative communications, correlation analysis

correlations of the channel coefficients [4] predicted by the SCM impact the predicted capacity and furthermore how those assumptions compare to measurement results in a real-world multicell deployment. For cooperative antenna techniques it is of interest to study the correlation of the fast fading channels which is done here for adjacent sector channels. Altogether it is found that SCM predicts an upper bound for the multicell correlations compared to our measurements. Hence we may conclude that simulation results based on the SCM provide a lower bound for the system performance.

I. INTRODUCTION

It has been shown in [1] that some slow fading parameters such as the shadow fading (SF) and angular spreads may be correlated if the base station antennas are closely spaced. This observation has led to an idealistic modelling assumption in the popular SCM [2] that the channels to adjacent sectors at the same site are derived from a common set of paths just weighted by the differently directed patterns of the sector antennas.

In recent research, cooperative base station techniques such as multiuser multiple-input multiple-output (MIMO) and joint transmission (JT) [3] are considered for application in future cellular systems. Therefore it is of great interest how the

II. MEASUREMENTS AND SCENARIOS

Two measurement scenarios are investigated in the central areas of Berlin and Dresden. Base station positions with heights, the measurement track and sector orientations are given in the Figures 1 and 2 and are described in detail in companion paper [5]. Position data have been recorded for each track using two independent global positioning system (GPS) receivers. The GPS data sets were averaged afterwards, fitted to the map and interpolated to get a more precise estimate of the terminal position. Large scale parameters such as the geometry factor (GF), single- and multicell delay spreads (DSs) as well as their correlations are accessible by aligning the data based on the position data.

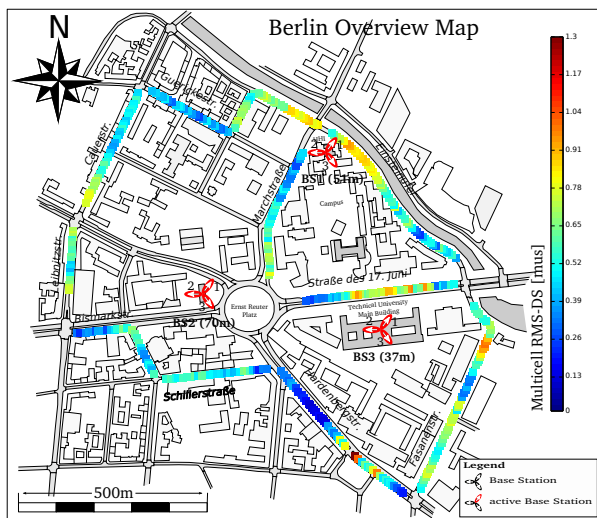


Figure 1. Map of the measurement area in Berlin. The multicell delay spread is plotted along the measurement track when all BS are transmitting coherently.

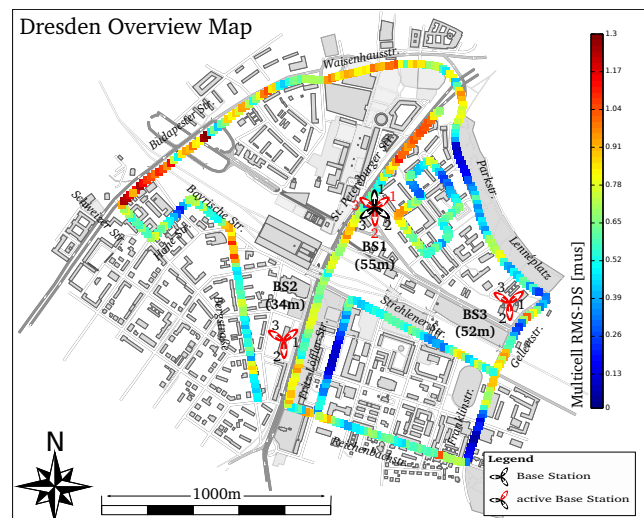


Figure 2. Map of the measurement area in Dresden. The multicell delay spread is plotted along the measurement track when all BS are transmitting coherently.

Table I
MEASUREMENT AND SIMULATION PARAMETERS

Parameter	Berlin	Dresden	Simulation
Center Frequency	2.53 GHz	2.53 GHz	2 GHz
Bandwidth (B)	20 MHz	21.25 MHz	30.72 Mhz
Time Windows	6.4 μ s	12.8 μ s	12.8 μ s
Carrier (N)	129	273	273
BS / Sectors	3 / 3	3(+1) / 3	3 / 3
Antennas (Tx)	PULA 8	X-POL	X-POL
Antennas (Rx)	PCUBE 5	PUCA 8	Omni
Vertical beam pattern	yes	yes	no
Inter Site Distance	500 m	750 m	750 m
Measurement Route	4500 m	8800 m	Random
Average Rx Velocity	15 km/h \approx 4.2 m/s		Random
Snapshots per Route	\approx 450.000		5000

The Berlin setup from August 2007 is composed of a 8 element polarized uniform linear array (PULA) at the BS and a polarized MIMO cube with 5 elements at the receiver. One sector covers an azimuth angle of 73° full width at half maximum (FWHM). In order to achieve a higher directivity in elevation, four patch elements have been coupled via a power divider resulting in a vertical FWHM of 37° . In Dresden, measurements were conducted in August 2008. Pre-commercial +18 dBi BS antennas (Kathrein 80010541) with two cross-polarized ports $\pm 45^\circ$ have been used. All sector antennas at one site have been fed like a single cross-polarized array with six input ports in the same switching sequence. This coherent recording makes it possible to study the fast fading correlation between the sectors as well. At the receiver, a polarized uniform circular array (PUCA) with 8 patch elements [6] has been used. Snapshot rates and recording times have been chosen to fulfill the channel sampling theorem.

Measurements with the same equipment but at other frequencies and with other antennas have been reported in [5–8]. The intention here is to extend the findings in [9] to a typical macro-cell deployment with three sectors at each site. The channel is measured at a carrier frequency of 2.53 GHz and a bandwidth of 20 MHz. These are typical parameters for the deployment of the 3G Long Term Evolution (3G-LTE) in Europe. For other measurement and simulation parameters refer to Table I.

III. DATA EVALUATION

A. Estimating the PDP

In mobile communications, the time domain impulse response (IR) is given as the sum of discrete channel taps

$$r(t) = \sum_{l=1}^L \alpha_l \cdot e^{j \cdot \phi_l} \cdot \delta(t - \tau_l) \quad (1)$$

where L is the total number taps and α_l , ϕ_l and τ_l are the amplitude, phase and delay of the l^{th} tap, respectively. The data, however, is obtained in frequency domain with a bandwidth $B = 20$ Mhz and a sampling rate of 320 MHz. Due to the bandwidth reduction and the equidistant sampling, the δ -pulse is broadened in time domain. Accurate values of α , ϕ and τ can be estimated more precisely with respect to the properties of the discrete Fourier transform (DFT). From the broadband frequency domain measurement data \mathbf{h} with

equidistant carriers, one can calculate a time domain IR \mathbf{r} with equidistant samples by an inverse discrete Fourier transform (IDFT)

$$r_m = \frac{1}{\sqrt{N}} \sum_{n=1}^N h_n \cdot e^{2\pi j \frac{(n-1)(m-1)}{N}} = \text{IDFT} \{ \mathbf{h} \} \quad (2)$$

where N is the number of carriers in the data. Each of the L taps in (1) can be estimated using a correlation approach. Therefore, we first define the Pearson product-moment correlation coefficient (PMCC) ρ between two series of N measurements \mathbf{a} and \mathbf{b}

$$\rho \{ \mathbf{a}, \mathbf{b} \} = \frac{\frac{1}{N} \sum_{n=1}^N a_n \cdot b_n^* - \frac{1}{N^2} \sum_{n=1}^N a_n \cdot \sum_{n=1}^N b_n^*}{\sqrt{\left(\sum_{n=1}^N \frac{|a_n|^2}{N} - \left| \sum_{n=1}^N \frac{a_n}{N} \right|^2 \right) \left(\sum_{n=1}^N \frac{|b_n|^2}{N} - \left| \sum_{n=1}^N \frac{b_n}{N} \right|^2 \right)}} \quad (3)$$

The maximum values α , ϕ and m of the strongest tap $|r_m|$ in the equidistant grid are used as a starting point for an iterative estimation process. From these values, a second vector is computed

$$\begin{aligned} f_f(n, m) = \mathbf{f}_f(m) &= \alpha \cdot e^{j \cdot \phi} \cdot e^{-2\pi j \frac{(n-1) \cdot m}{N}} \\ \mathbf{f}(m) &= \text{IDFT} \{ \mathbf{f}_f(m) \} \end{aligned} \quad (4)$$

This vector is now used as a correlator to calculate $\rho \{ \mathbf{r}, \mathbf{f}(m) \}$ in (3) with the free parameter m . Note that m can now be any real number between 0 and $N - 1$. The PMCC is maximal at the exact position m_{opt} of the tap. The maximum can be calculated using well know numerical methods. The absolute time of arrival τ then results from

$$\tau = \frac{m_{\text{opt}}}{B} \quad (5)$$

The second step is to determine the optimal phase angle ϕ for the already given position m_{opt} . Again, this can be solved numerically. The process is started by calculating $\mathbf{f}(\phi)$ similar to (4) but with fixed m and α . Subtracting \mathbf{f} from \mathbf{r} removes the estimated tap from the IR, but only for the correct settings ϕ and α . $\rho \{ \mathbf{r} - \mathbf{f}(\phi), \mathbf{f}(\phi) \}$ becomes minimal for the optimal

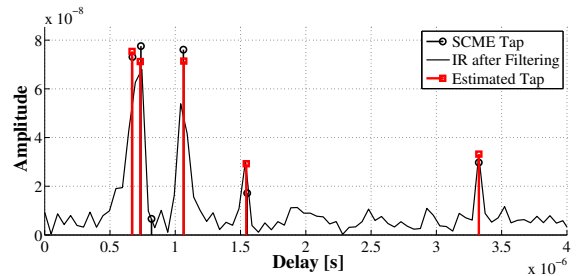


Figure 3. Example of the PDP estimation: The black taps were calculated by the SCM. The IR (black line) was then calculated by reducing the bandwidth to 20 MHz and adding noise so that the SNR was 5 dB. The iterative estimator could detect 5 of the 6 taps with high precision (red bars) although they were not distinguishable in the IR anymore.

setting of ϕ and zero for both, the optimal ϕ and the optimal α . These parameters can be found by solving

$$\phi_{\text{opt}} = \arg \min_{\phi} \rho \{ \mathbf{r} - \mathbf{f}(\phi), \mathbf{f}(m_{\text{opt}}, \phi) \} \quad (6)$$

$$\alpha_{\text{opt}} = \arg \min_{\alpha} \rho \{ \mathbf{r} - \mathbf{f}(\alpha), \mathbf{f}(m_{\text{opt}}, \phi_{\text{opt}}, \alpha) \} \quad (7)$$

where for (6) the parameters m and α , and for (7) m and ϕ are kept fixed, respectively. When all three parameter have been estimated, the strongest tap is removed from the impulse response

$$\mathbf{r}_{\text{new}} = \mathbf{r} - \mathbf{f}(m_{\text{opt}}, \phi_{\text{opt}}, \alpha_{\text{opt}}) \quad (8)$$

and the entire process is repeated for the next tap. The algorithm terminates when a stop criterium is reached

$$\frac{\alpha^2}{\sum_{n=1}^N |h_{tn}|^2} < P_{\text{lim}} \quad (9)$$

In that case, the last detected tap is discarded. P_{lim} is set according to the expected noise variance. If there is only noise left in the IR, the denominator in (9) describes the average noise power. Since the power of white noise follows a Chi-Squared distribution, it's variance is twice as large as it's mean value. Setting $P_{\text{lim}} = 8$ ensures that the detected peak is part of the signal space with 99.9% probability.

The entire detection algorithm is a suboptimal estimation process which does not need any a-priori information about the number of taps in the IR. It is similar to the V-BLAST algorithm in MIMO communications [10] where several data streams are also detected iteratively. Another iterative extension as described in [11] can be applied to further improve the results. Alternatively, with the known taps, maximum likelihood (ML) estimates as used by RiMAX [12] can be an extension.

B. Shadow Fading

The shadow fading, commonly modelled as log-normal shadowing reflects the fact that several terminals at the same distance to the BS have a different environment [13]. This leads to a random (log-normal) distributed distortion of the distance dependent path loss. The instantaneous path loss can be estimated from the measurement data by averaging all signal components over all transmit and receive antennas of one sector

$$P_i = \frac{1}{n_t n_r} \cdot \sum_{i=1}^{n_t} \sum_{j=1}^{n_r} P_t^{ij} \quad (10)$$

where P_t is the total power of a power delay profile (PDP) and i, j are the indices of the transmit and receive antenna element.

$$P_t = \sum_{l=1}^L \alpha_l^2 \quad (11)$$

Since the receive antenna is a circular setup of cross-polarized (directional) patch elements, averaging the received power over all receive (Rx) antennas in (10) is comparable to a dipole antenna where the effects of polarization have been removed. Also note that the use of extracted taps in (11) leads to a

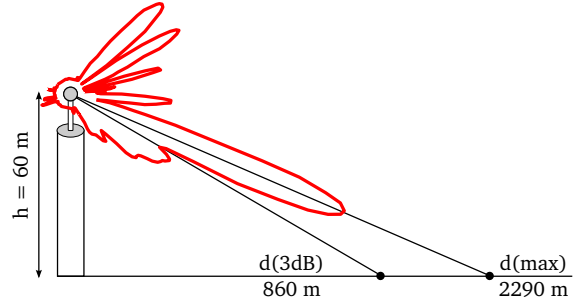


Figure 4. With 1.5° tilt and a antenna height of 60 m, the main beam of the transmit antenna reaches the ground in a distance of 2290 m whereas less power is received close to the BS. The 3 dB point of the main lobe reaches the ground in 860 m distance from the BS.

significant noise reduction. Instantaneous values P_i within an area of 5 m are then averaged to increase the precision of the estimate. To obtain the SF, one first has to calculate the distance dependent path loss (PL) normally modelled as

$$PL(d) = PL(d_0) + A \cdot \log_{10}(d_{\text{km}}) \quad (12)$$

$PL(d_0)$ is the PL (in dB) at a reference distance d_0 and A is the path loss exponent which describes the change of the PL when going to distance d . In our case, d_0 is set to 1 km.

Our measurements were conducted with highly directional antennas. Depending on the angle of departure (AoD) at the BS and the angle of arrival (AoA) at the receiver, multipath components are weighted by the corresponding points in the beam patterns of the antennas. To simulate omnidirectional coverage in azimuth direction, all three values of P_i representing the three sectors of a BS are summed up to P_s . This approach leaves the high directivity in elevation. As shown in Fig. 4, the vertical beam pattern of the transmit antenna increases the received power at a certain distance from the BS and lowers the power close to the BS. This effect will significantly reduce the path loss exponent A yet it is rather typical for cellular deployments. We therefore refer to distance dependent component as effective PL where the effects of antenna-patterns have not been removed.

With these two modifications (the noise reduction due to tap extraction and using the sumpower of all sectors of one BS), one would estimate $P_d(d)$ and A by a least squares fit of all values P_s against distance d and determine the shadow fading by a Gaussian fit of the residual components at distance d (see [14]).

C. Delay Parameters

The temporal dispersion of the channel is typically described by two parameters [13]: the root mean square (RMS) delay spread and the maximum excess delay. The RMS delay spread is defined as the second central moment of the noise free PDP

$$\sigma_\tau = \sqrt{\tau^2 - (\bar{\tau})^2} \approx \sqrt{\sum_{l=1}^L \frac{\alpha_l^2}{P_t} \cdot \tau_l^2 - \tau_m^2} \quad (13)$$

with τ_l as the delay- and α_l^2 the power of the l^{th} tap. τ_m is the mean delay

$$\bar{\tau} \approx \tau_m = \sum_{l=1}^L \frac{\alpha_l^2}{P_t} \cdot \tau_l \quad (14)$$

The excess delay describes the time span where a certain percentage p of signal energy arrives at the receiver. We calculate it using the normalized cumulative sum of the PDP

$$P_{cs}(\tau) = \frac{\int_0^\tau p(t)dt}{\int_0^\infty p(t)dt} \approx \frac{\sum_0^\tau p(t_p)}{\sum_0^L p(t_p)} \quad (15)$$

and define the 99% excess delay as the time between the 1- and the 99-percentiles of $P_{cs}(t)$. Traces where there are not enough taps detected above the noise floor are excluded from the evaluation.

D. Fast Fading correlation

Due to the coherent measurement setup in Dresden, fast fading correlations using the PMCC (3) of different sectors of the same site can be computed. The channel vector $\mathbf{H}^{(a)}$ contains N directly measured complex valued frequency bins h_a from one transmit (Tx)-element at a given sector to one specific Rx element at the receive array. No averaging is applied. Vice versa, $\mathbf{H}^{(b)}$ contains the frequency response to another sector but for the same Rx element. The PMCC is computed from frequency domain measurement data for different sectors at the same site using the same polarization at both sector antennas. A high value of $|\rho\{\mathbf{H}^{(a)}, \mathbf{H}^{(b)}\}|$ indicates that the communication channels to two BS at a given mobile terminal (MT) position are correlated.

IV. RESULTS

A. Shadow Fading

In Dresden, the effective path loss exponent is estimated to $A = 1.85$ and the standard derivation of the SF is $\sigma_{SF} = 9.7$ dB. The low value of A can be explained with the high directivity of the sector antenna. Due to the elevation pattern of the antenna, less power is radiated close to the BS and the main beam hits the ground in about 860 m distance (see Fig. 4.). This leads to a significantly lower PL exponent even with non line of sight (NLOS) propagation. A major drawback in the SCM is that vertical beampatterns and downtilts are not part of the current implementation [2]. These parameters play a significant role in the propagation characteristics of a multicellular system. In Berlin, the effective PL exponent is estimated to $A = 1.63$ and the SF has $\sigma_{SF} = 8.6$ dB (see Fig. 5). The SCM assumes a σ_{SF} of 8 dB, which agrees well with the measurement results.

The cross-correlations of the SF are listed in Table II. As expected, the correlation of BS1a and BS1b in Dresden is high (0.76) since both BSs are situated at the same site. The average inter-site cross correlation in both testbeds is 0.23 when taking only the grey shaded values from Table II. Note that this value has a significant standard deviation of 0.17. In comparison, the SCM assumes site-to-site SF correlation of 0.5 which is about twice as high as in our measurement scenario.

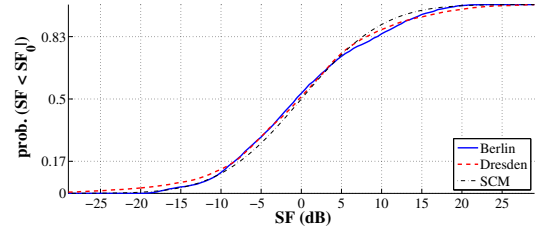


Figure 5. Distribution of the shadow fading in both testbeds. Standard derivations were 8.6 dB in Berlin and 9.7 dB in Dresden.

Table II
INTERSITE CORRELATION OF THE SHADOW FADING

	Berlin			Dresden			
	BS1	BS2	BS3	BS1a	BS1b	BS2	BS3
BS1	1	0.05	0.35	BS1a	0.76	0.26	0.17
BS2		1	0.53	BS1b	1	0.12	0.02
BS3			1	BS2		1	0.33

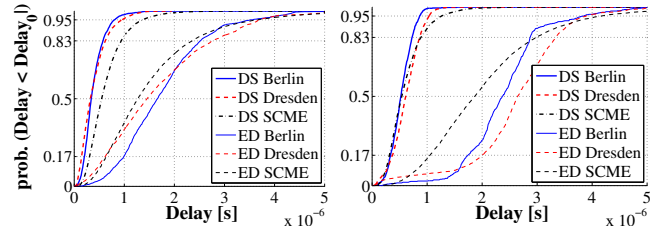


Figure 6. Distribution of the RMS delay spread (DS) and the 99% excess delay in Berlin (blue, solid line) and Dresden (red, dashed line). The left figure shows the per-BS delay spread and the right figure the multicell delay spread. Results from the SCME are shown as black dashed line.

Table III
DELAY PARAMETERS OVERVIEW

	Single-Site Delays				Multicell Delays			
	DS.5	DS.95	ED.5	ED.95	DS.5	DS.95	ED.5	ED.95
Berlin	0.34	0.81	1.67	3.54	0.52	0.86	2.37	3.85
Dresden	0.32	0.95	1.45	3.69	0.61	1.04	2.65	3.89
SCME	0.45	0.96	1.06	2.38	0.44	0.92	1.50	2.75

Table IV
INTERSITE CORRELATION OF THE RMS DELAY SPREAD

	Berlin			Dresden			
	BS1	BS2	BS3	BS1a	BS1b	BS2	BS3
BS1	1	-0.14	-0.08	BS1a	0.47	0.10	0.01
BS2		1	-0.13	BS1b	1	-0.02	-0.16
BS3			1	BS2		1	0.22

Table V
INTERSECTOR CORRELATION OF THE RMS DELAY SPREAD

Sec.	Berlin			Dresden			
	BS1	BS2	BS3	BS1a	BS1b	BS2	BS3
1-2	0.10	0.09	-0.07	0.04	0.21	0.21	0.04
1-3	0.41	0.58	0.15	-0.06	0.14	0.25	0.05
2-3	-0.08	0.30	0.16	0.14	0.05	0.43	0.01

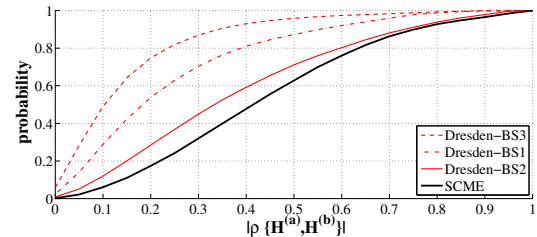


Figure 7. CDFs for the fast fading correlation in Dresden (red curves) compared with the result of the SCM simulation.

B. Delay Parameters

Results on the RMS delay spreads and the excess delays are given in Fig. 6. The left figure shows the cumulative distribution functions (CDFs) for independent BSs where the taps from all three sectors have been merged in order to simulate omnidirectional coverage. The median single site RMS-DS for both scenarios is about $\sigma_{DS} = 0.33 \mu\text{s}$. This value rises to $0.55 \mu\text{s}$ when using cooperative transmission. The SCM assumes a σ_{DS} of $0.65 \mu\text{s}$ without taking the effect of the beampatterns into account. Using the simulated channels with horizontal beampatterns applied, a $\sigma_{DS} = 0.55 \mu\text{s}$ is predicted which exceeds the measured value by 60%.

The corresponding 95% quantile is $0.88 \mu\text{s}$ for the single-site and $0.95 \mu\text{s}$ for the multicell deployment. In general, multicell distributions of the delay parameters are steeper. The same holds for the 99% excess delay. All parameters are listed in Tab. III. In both testbeds, the 0.95 percentiles of the multicell distributions only exceed their single-site counterparts by 8% and the maximum value is less than $5 \mu\text{s}$ in 99% of the cases.

The correlations of the RMS delay spreads at different sites in both scenarios are listed in Table IV. On average, inter-site delay spreads are mutually uncorrelated. ($\bar{\rho}=0.02$). When considering only different sectors of the same BS, the average correlation rises to $\bar{\rho}=0.17$. Note that for this case, the effect of the beampatterns at the transmit antenna have not been removed and that BS1 in Berlin and BS3 in Dresden have been excluded from the statistics because there were not enough values to calculate the PMCC (3) for different sectors. All values for the intersector correlation of the DS are listed in Table V where columns represent the BS and rows represent the sector combination.

C. Fast Fading Correlation

Channels for evaluations of the frequency fading correlation have been selected for each two sectors of one BS when the received power in both sectors was more than -95 dBm . That selection has been done for all Rx elements and all positions along the 8.8 km measurement track in Dresden. All values of $|\rho\{\mathbf{H}^{(a)}, \mathbf{H}^{(b)}\}|$ then form a CDF for each BS as depicted in Fig. 7. It seems that there is a strong dependence on the placement of the antennas. The antennas were on different edges of the roof for BS1 and BS3 ($\approx 20 \text{ m}$ apart) but within 3 wavelengths for BS2. In this case the correlation is highest and 20% of the terminal positions have a $|\rho\{\mathbf{H}^{(a)}, \mathbf{H}^{(b)}\}| > 0.6$. The comparison with the SCM only agrees with the measurements when the antennas are close together which is almost the case for BS2. So far, variable spacings between the antennas of different sectors at one BS are not included in the SCM. The correlation is therefore overestimated, in particular when the sector antenna deployment is distributed rather than on the same mast.

V. CONCLUSIONS

Data from two multicell measurement campaigns in Dresden and in Berlin have been evaluated in order to verify

common modelling assumptions in the popular spatial channel model (SCM). Data preprocessing was done by an iterative estimation process which decomposes the measured frequency response of the channel into a set of channel filter taps. Based on these taps, path loss (PL), shadow fading (SF), delay spreads (DSs) and excess delays (EDs) as well as their correlations have been calculated. These results have been compared to simulated channels from the SCM. In general, the SCM is in good agreement with the measurements. Large scale parameters are well modelled but the SCM assumes higher correlations between the channel parameters from different sites. Simulation results regarding the throughput of a cooperative cellular system can therefore be considered as a lower bound.

ACKNOWLEDGMENTS

The authors wish to thank the German Ministry of Education and Research (BMBF) for financial support in the national collaborative projects 3GeT and EASY-C. Furthermore we thank our partners Actix, Alcatel-Lucent, Deutsche Telekom, Ericsson, Kathrein, Qualcomm, TU Dresden and Vodafone for financial support of the campaign in Dresden. Many thanks to U. Krüger, A. Brylka, T. Wirth, Y. Hadisusanto, M. Mehlhose, S. Schiffermüller, K. Börner (all from HHI) and S. Warzügel (MEDAV) for assistance during the measurements.

REFERENCES

- [1] N. Jaldén, P. Zetterberg, B. Ottersten, and L. Garcia, "Inter-and intrasite correlations of large-scale parameters from macrocellular measurements at 1800 MHz," *EURASIP JWCN*, vol. 2007, no. 3, 2007.
- [2] 3GPP TR 25.996 v7.0.0, "Spatial channel model for multiple input multiple output (MIMO) simulations," Tech. Rep., 6 2007.
- [3] P. Baier, M. Meurer, T. Weber, and H. Troger, "Joint transmission (JT), an alternative rationale for the downlink of time division CDMA using multi-element transmit antennas," *Proc. IEEE ISSSTA '00*, 2000.
- [4] P. Kyritsi, D. Cox, R. Valenzuela, and P. Wolniansky, "Correlation analysis based on MIMO channel measurements in an indoor environment," *IEEE J. Sel. Areas Commun.*, vol. 21, pp. 713–720, 2003.
- [5] S. Jaeckel, L. Thiele, A. Brylka, L. Jiang, and V. Jungnickel, "Intercell interference measured in urban areas," *Proc. IEEE ICC '09 (accepted)*, 2009.
- [6] R. Thomä, D. Hampicke, A. Richter, G. Sommerkorn, and U. Trautwein, "MIMO vector channel sounder measurement for smart antenna system evaluation," *Europ. Trans. Telecommun.*, vol. 12, no. 5, pp. 427–438, 2001.
- [7] M. Landmann, K. Sivasondhivat, J. Takada, and R. Thomä, "Polarisation behaviour of discrete multipath and diffuse scattering in urban environments at 4.5 GHz," *EURASIP JWCN*, vol. 2007, no. 1, pp. 60–71, 2007.
- [8] V. Jungnickel, S. Jaeckel, L. Thiele, L. Jiang, U. Krüger, A. Brylka, and C. Helmolt, "Capacity measurements in a cooperative multicell MIMO network," *IEEE Trans. Veh. Technol. (accepted)*, 2009.
- [9] L. Thiele and V. Jungnickel, "Out-of-cell channel statistics at 5.2 GHz," *Proc. EuCAP '06*, November 2006.
- [10] P. W. Wolniansky, G. J. Foschini, and G. D. Golden, "V-blast: An architecture for realizing very high data rates over the rich-scattering wireless channel," *Invited Conference Papers Proc. ISSSE-98 in Pisa*, 1998.
- [11] A. Sezgin, E. Jorswieck, and V. Jungnickel, "Maximum diversity detection for layered space-time codes," *Proc. IEEE VTC '03 Spring*, vol. 2, pp. 833–837, 2003.
- [12] A. Richter, M. Landmann, and R. S. Thomä, "RIMAX - a flexible algorithm for channel parameter estimation from channel sounding measurements," *COST 273 TD(04) 045*, 2004.
- [13] T. Rappaport, *Wireless Communications. Principles and Practice*, 2nd ed. Prentice Hall, 2002.
- [14] A. Algans, K. Pedersen, and P. Mogensen, "Experimental analysis of the joint statistical properties of azimuth spread, delay spread, and shadow fading," *IEEE J. Sel. Areas Commun.*, vol. 20, no. 3, pp. 523–531, 2002.